UNIVERSITÄT AUGSBURG
Universitätsbibliothek

OPEN ACCESS
OPUS AUGSBURG

Characterizing bladder filling physiology with long-axial-FOV dynamic PET/CT

Varvara Kondratyeva, Lukas Förner, Kartikay Tehlan, Melina Wördehoff, Axel Rominger, Kuangyu Shi, Thomas Wendler

Angaben zur Veröffentlichung / Publication details:

Kondratyeva, Varvara, Lukas Förner, Kartikay Tehlan, Melina Wördehoff, Axel Rominger, Kuangyu Shi, and Thomas Wendler. 2026. "Characterizing bladder filling physiology with long-axial-FOV dynamic PET/CT." *Current Directions in Biomedical Engineering* 12 (1): 255–58. https://doi.org/10.1515/cdbme-2026-0165.

Nutzungsbedingungen / Terms of use:

CC BY 4.0

Dieses Dokument wird unter folgenden Bedingungen zur Verfügung gestellt: / This document is made available under these conditions:
CC-BY 4.0: Creative Commons: Namensnennung
Weitere Informationen finden Sie unter: / For more information see:
https://creativecommons.org/licenses/by/4.0/deed.de

Varvara Kondratyeva, Lukas Förner*, Kartikay Tehlan, Melina Wördehoff, Axel Rominger, Kuangyu Shi, and Thomas Wendler

Characterizing Bladder Filling Physiology with Long-Axial-FOV Dynamic PET/CT

https://doi.org/10.1515/cdbme-2026-0165

Abstract:
Bladder filling during dynamic long-axial field-of-view (FOV) [^{18}F]Fluorodeoxyglucose ([^{18}F]FDG) positron emission tomography (PET) imaging leads to motion-related misalignment between frames. As a first step toward this misalignment correction, we track urinary bladder expansion and frame-by-frame shape changes. Starting from the final PET frame, our algorithm applies intensity normalization, distribution-based correction, and region growing to estimate bladder volume over time. Compared to automated multi-organ segmentation frameworks, namely TotalSegmentator and MOOSE, the proposed PET-based method provides more accurate and physiologically plausible segmentations. Using our final-frame masks as reference, Dice-Sørensen coefficients were 0.40 ± 0.37 for TotalSegmentator and 0.70 ± 0.26 for MOOSE. In 21 successfully segmented patients, bladder volume increased approximately linearly over time ($R^2 = 0.94[0.88, 0.97]$), while fractional anisotropy decreased (Spearman's $\rho = -0.86[-0.96, -0.61]$), indicating a trend toward a more spherical bladder shape during filling. The bladder was typically no longer traceable at frame 40 (4-4.5 min post-injection).

Keywords: bladder, 3D+t image segmentation, organ displacement, dynamic PET/CT, FDG, tracking

Varvara Kondratyeva, Kartikay Tehlan, Thomas Wendler, Lukas Förner, Chair for Computer-Aided Medical Procedures and Augmented Reality, Technical University of Munich, Germany
***Corresponding author: Lukas Förner,** Dept. of Diagnostic and Interventional Radiology and Neuroradiology, University Hospital Augsburg, Germany, e-mail: lukas.foerner@uk-augsburg.de
Kartikay Tehlan, Melina Wördehoff, Thomas Wendler, Varvara Kondratyeva, Dept. of Diagnostic and Interventional Radiology and Neuroradiology, University Hospital Augsburg, Germany
Kartikay Tehlan, Melina Wördehoff, Thomas Wendler, Lukas Förner, Digital Medicine, University Hospital Augsburg, Augsburg, Germany
Kartikay Tehlan, Melina Wördehoff, Thomas Wendler, Lukas Förner, Bavarian Center for Cancer Research (BZKF) Augsburg, Germany
Axel Rominger, Kuangyu Shi, Dept. of Nuclear Medicine, Inselspital Bern, Switzerland
Thomas Wendler, Center for Advanced Analytics and Predictive Sciences, University of Augsburg, Germany

1 Introduction

Dynamic PET imaging is typically used for kinetic parameter estimation, particularly to detect early recurrence or characterize unspecific uptake [1, 2]. Yet, during imaging, the urinary bladder accumulates tracer excreted by the kidneys, resulting in an expansion that displaces adjacent structures, such as the intestines, prostate, and kidneys. As computed tomography (CT) scanning typically occurs after the PET acquisition, the bladder is often delineated therein at its largest volume, resulting in positional inconsistencies for other organs across the PET frames. Reducing this misalignment would require reliable temporal information about bladder expansion and shape changes. Therefore, as a first step toward future motion-correction approaches, we track the urinary bladder expansion and evaluate its frame-by-frame shape without additional interventions such as catheterization.

2 Materials and Methods

2.1 Data

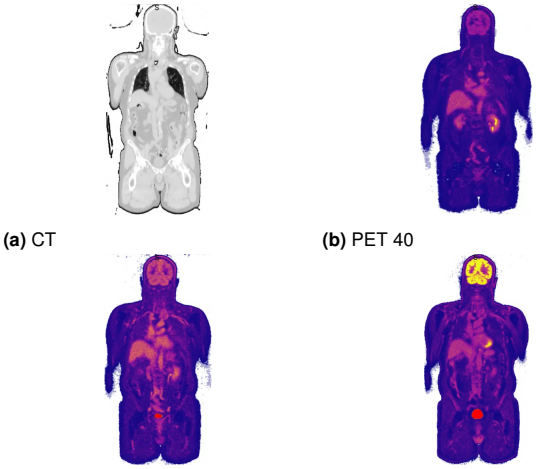
The dataset consists of 23 patients with various primary tumor types who underwent dynamic PET imaging using a Siemens Biograph Vision Quadra long-field-of-view PET/CT device. Average injected activity amounted to 235 ± 51 MBq of [^{18}F]FDG. Dynamic PET lasted 65 minutes for all patients totaling 62 frames with varying durations: 2 × 10 s, 30 × 2 s, 4 × 10 s, 8 × 30 s, 4 × 60 s, 5 × 120 s and 9 × 300 s (Figure 1).

A low-dose CT scan immediately followed the PET acquisition (voltage: 120 kV, tube current: 25 mA). PET and CT image resolution were 1.65 × 1.65 × 1.65 mm³, and 1.5 × 1.5 × 1.6 mm³ respectively. CT and PET frames were resampled to an isotropic voxel size of 2.5 mm.

2.2 CT-based bladder segmentation

Established multi-organ segmentation frameworks, such as TotalSegmentator (TS) [3] and MOOSE [4], are widely used and have shown particularly strong performance in CT. We therefore first evaluated this approach: the tools were applied

Open Access. © 2026 The Author(s), published by De Gruyter. This work is licensed under the Creative Commons Attribution 4.0 License.



(a) CT **(b)** PET 40 **(c)** PET 45 **(d)** PET 61

Fig. 1: PET coronal views with the urinary bladder mask (red) at frames 40 (4-4.5 min), 45 (7-8 min), and 61 (60-65 min post-injection).

to the CT, the resulting mask transferred to the last PET frame (frame 61), and propagated backwards to the first frame (frame 0).

2.3 PET-based bladder segmentation

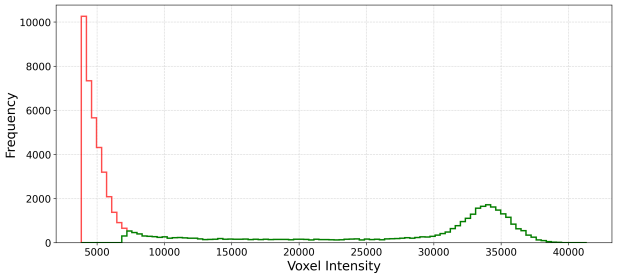


(a) MOOSE mask (frame 61). **(b)** TS mask (frame 61).

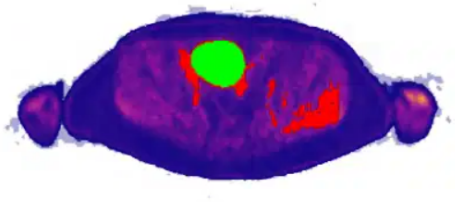
Fig. 2: Patient 2, illustrating limited segmentation accuracy. The bladder mask produced by the tool (red) is overlaid on a PET axial slice (frame 61, 60–65 min); the high FDG uptake marking the true bladder (yellow) extends well beyond it.

Because of the low-contrast between the bladder and the surrounding soft tissue, CT-based segmentation may be unreliable (Figure 2). We therefore propose incorporating the PET information already at the last frame, using the CT-based segmentation only as prompt. Specifically, the bladder masks produced by TS were used to crop the PET image to an approximate region (cube) in which the bladder is expected be to lie for any patient.

For this final PET frame, voxel intensities within the cropped region were normalized to $[0, 1]$ – making the algorithm patient-independent – then thresholded (threshold = 0.1) and refined by removing high-frequency distribution tails inconsistent with homogeneous urinary activity (Figure 3a). The resulting mask was propagated backwards through the dynamic PET frames using confidence-connected region growing with 6-connectivity, and propagation was stopped once the bladder was no longer visually traceable.



(a) PET 61: initial (red) and corrected (green) intensity histograms.



(b) PET 61: initial (red) and corrected (green) masks.

Fig. 3: Patient 2, mask correction applied on last PET image (frame 61, 60-65 min).

To refine the initial mask, we analyze the histogram of voxel intensities within it (see Figure 3). The histogram is bimodal: a tall, narrow spike at low intensity, corresponding to background and partial-volume voxels admitted by the permissive 0.1 threshold, and a broad mode at high intensity, corresponding to the homogeneous high uptake of the bladder. We identify the high-intensity mode as the bladder and compute its mean bin frequency μ_{freq}. The low-intensity spike is then removed: starting from the low-intensity end, we discard the contiguous bins whose frequency exceeds $\mu_{\text{freq}}/2$, retaining the remaining high-intensity voxels as the refined bladder mask.

The intensity histogram of the last PET frame visually follows a normal distribution, but this pattern becomes progressively less pronounced in earlier frames, owing to the progressively smaller amount of accumulated tracer. As a result, the threshold-based mask increasingly underestimates the bladder volume in earlier frames.

To address this, we apply region growing using the SimpleITK [5] ConfidenceConnectedImageFilter. Starting from the existing mask as seed voxels, the algorithm computes the mean (μ) and standard deviation (σ) of voxel intensities in a $3 \times 3 \times 3$ neighborhood around each seed. A neighboring voxel x with intensity $I(x)$ is added to the region if it satisfies the in-

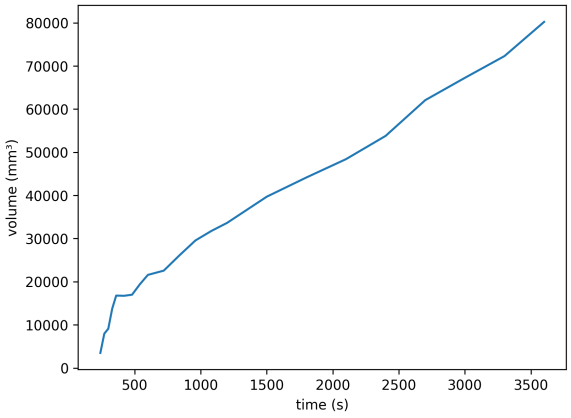
tensity similarity criterion: $|I(x) - \mu_{\text{region}}| \leq m \cdot \sigma_{\text{region}}$, where μ_{region} and σ_{region} are the mean and standard deviation of the intensities in the current region and m is a frame-specific multiplier setting the width of the accepted intensity band. We define $m = (\mu_{\text{region}} - min_{\text{region}})/\sigma_{\text{region}}$, where min_{region} is the minimum intensity in the region. Vicinity is defined by face-adjacent (6-) connectivity in 3D.

The algorithm yields one segmentation mask per PET frame, proceeding backwards from the last frame and stopping once the bladder is no longer visible – typically at frame 40 (4-4.5 min post-injection) in our dataset.

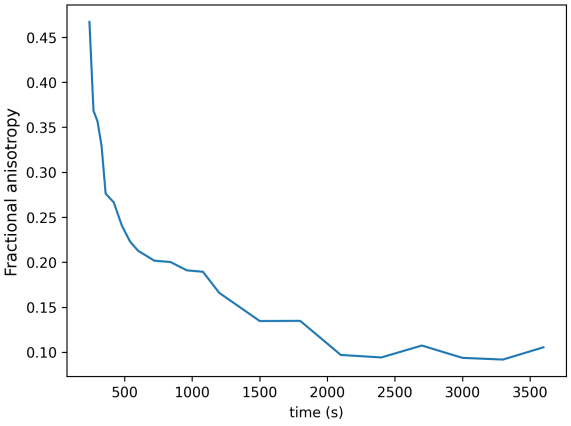
For quantitative evaluation, we studied the dynamics of the bladder shape and volume over time. The volume is computed by counting the segmented voxels and multiplying by the voxel volume. We adopt fractional anisotropy (FA) as the shape descriptor which agreed with standard sphericity and the principal-axis eigenvalue ratios on our data:

$$\text{FA} = \sqrt{\frac{3}{2}} \frac{\sqrt{(\lambda_1 - \bar{\lambda})^2 + (\lambda_2 - \bar{\lambda})^2 + (\lambda_3 - \bar{\lambda})^2}}{\sqrt{\lambda_1^2 + \lambda_2^2 + \lambda_3^2}} \quad (1)$$

where λ_i are the eigenvalues of a PCA over the coordinates of all mask voxels and $\bar{\lambda} = (\lambda_1 + \lambda_2 + \lambda_3)/3$. Although fractional anisotropy is most familiar from diffusion MRI, here it is applied purely as an eigenvalue-based descriptor of shape anisotropy. The eigenvalues describe the spatial spread of the bladder along its three principal axes, so FA characterizes how that spread is distributed: FA = 0 corresponds to equal spread along all axes (a spherical shape), while values toward 1 indicate increasing elongation or flattening.



(a) Bladder volume increases approximately linearly over time.



(b) Fractional anisotropy decreases over time.

Fig. 4: Bladder volume (a) and fractional anisotropy (b) over time for example patient 1.

3 Results

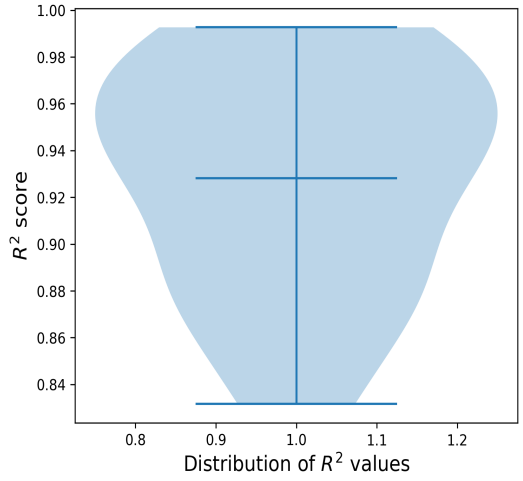
Expert review indicated good qualitative segmentation performance. In 2 of 23 cases, the algorithm failed to segment the bladder, owing to anomalous uptake in the surrounding region — specifically, tumor tissue close to the bladder. For the remaining 21 patients, temporal trends were evaluated per patient by correlating each quantitative measure with elapsed acquisition time across that patient's segmented frames. Bladder volume showed a strong, approximately linear increase over time (coefficient of determination $R^2 = 0.94[0.88, 0.97]$; Figures 4a, 5a). Fractional anisotropy showed a decreasing trend, indicating that the bladder became more spherical during filling, though this trend was not necessarily linear. We therefore report two per-patient correlations: Pearson (r) to capture the linear component, and Spearman (ρ) to capture monotonic, potentially non-linear behavior; the gap between them serves as an indicator of non-linearity in the shape evolution. This yielded $r = -0.82[-0.96, -0.39]$ (Fisher-averaged) and $\rho = -0.86[-0.96, -0.61]$ (Figures 4b and 5b).

To assess the existing tools, we computed Dice–Sørensen coefficients (DSC) using the masks generated by our method as the reference segmentation, obtaining 0.40 ± 0.37 for TS and 0.70 ± 0.26 for MOOSE on the last PET frame across all patients.

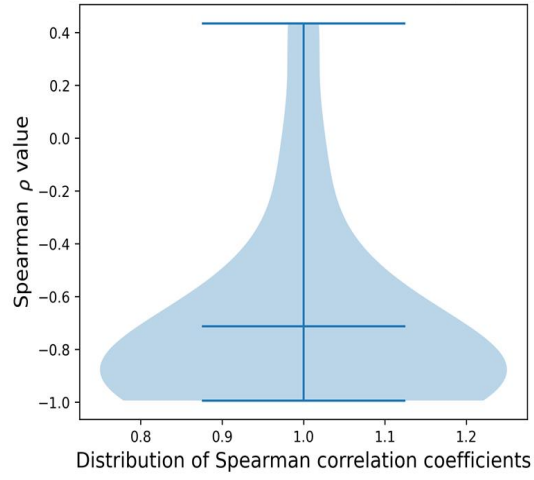
4 Discussion

To the best of our knowledge, no previous study has analyzed changes in bladder shape in the context of dynamic PET. This is notable, as many radioactive tracers are excreted by the kidneys and thus accumulate in the bladder during acquisition.

We found that the established multi-organ tools produced bladder masks of insufficient accuracy. This may be because such tools are designed for many organs at once and are there-



(a) Coefficient of determination R^2 for volume change (linear relation).



(b) Spearman correlation ρ for anisotropy (monotonic relation).

Fig. 5: Per-patient temporal-trend measures across 21 patients: R^2 for volume (a) and Spearman ρ for fractional anisotropy (b).

fore not optimized for a single target, or because the low bladder–soft-tissue contrast is itself challenging. In our cohort, TS [3] and MOOSE [4] showed poor agreement with our segmentations (Figure 2).

The algorithm was not applicable to the 2 patients with tumor uptake close to the bladder. In these cases, FDG accumulates in the cancerous tissue as strongly as in the bladder, rendering the two inseparable on the PET frames, so the region growing erroneously merges cancerous regions into the bladder mask.

The main limitation of our analysis is its semi-quantitative nature, due to the absence of ground-truth segmentations. Nevertheless, the expert assessment of the masks and the observed trends — approximately linear volume growth and a monotonic anisotropy decrease — are consistent with textbook anatomy and physiology.

In summary, we developed and evaluated a custom algorithm for urinary bladder segmentation in dynamic FDG PET. Unlike the established multi-organ tools, which showed limited accuracy for bladder delineation, our method traces the bladder across multiple PET frames, enabling reliable tracking of its expansion and thereby reducing potential misalignment of adjacent organ masks.

Future work will focus on deepening the shape and volume analysis, exploiting CT information to handle anomalous uptake near the bladder, and integrating this into motion compensation for kinetic parameter estimation.

Author Statement

Research funding: This research was partially funded by the Intramural Research Funding Grants “MultiPro” and “AI-driven Longitudinal Lesion Tracking” of the Faculty of Medicine, University of Augsburg, the Bavarian Center for Cancer Research as part of the Lighthouse “Local Therapies”, as well as by the Bavarian Ministry of Economic Affairs, Regional Development and Energy (StMWi) under grant number DIK-2310-0004// DIK0556/02. **Conflict of interest**: Authors state no conflict of interest. **Informed consent**: Informed consent has been obtained from all individuals included in this study. **Ethical approval**: The research related to human use complies with all the relevant national regulations, institutional policies and was performed in accordance with the tenets of the Helsinki Declaration, and has been approved by the authors’ institutional review board.

References

[1] Carson RE. Tracer Kinetic Modeling in PET. In: Bailey DL, Townsend DW, Valk PE, Maisey MN, editors. Positron Emission Tomography: Basic Sciences. London: Springer London; 2005. p. 127-59.

[2] Pantel AR, Viswanath V, Muzi M, Doot RK, Mankoff DA. Principles of Tracer Kinetic Analysis in Oncology, Part I: Principles and Overview of Methodology. Journal of Nuclear Medicine. 2022;63(3):342-52.

[3] Wasserthal J, Breit HC, Meyer MT, Pradella M, Hinck D, Sauter AW, et al. TotalSegmentator: Robust Segmentation of 104 Anatomic Structures in CT Images. Radiology: Artificial Intelligence. 2023;5(5):e230024.

[4] Ferrara D, Pires M, Gutschmayer S, Yu J, Abdelhafez YG, Abenavoli E, et al. Sharing a whole-/total-body [18F]FDG-PET/CT dataset with CT-derived segmentations: an ENHANCE.PET initiative. Scientific Data. 2026;13(1):869.

[5] Lowekamp BC, Chen DT, Ibáñez L, Blezek D. The Design of SimpleITK. Frontiers in Neuroinformatics. 2013;7:45.